

Dependence of DNA Persistence Length on Ionic Strength and Ion Type

Sébastien Guilbaud,^{1,‡} Laurence Salomé,¹ Nicolas Destainville,² Manoel Manghi,^{2,*} and Catherine Tardin^{1,†}

¹*Institut de Pharmacologie et de Biologie Structurale, Université de Toulouse, CNRS, UPS, 31 077 Toulouse, France*

²*Laboratoire de Physique Théorique (IRSAMC), Université de Toulouse, CNRS, UPS, 31 062 Toulouse, France*



(Received 28 September 2018; published 18 January 2019)

Even though the persistence length L_P of double-stranded DNA plays a pivotal role in cell biology and nanotechnologies, its dependence on ionic strength I lacks a consensual description. Using a high-throughput single-molecule technique and statistical physics modeling, we measure L_P in the presence of monovalent (Li^+ , Na^+ , K^+) and divalent (Mg^{2+} , Ca^{2+}) metallic and alkyl ammonium ions, over a large range $0.5 \text{ mM} \leq I \leq 5 \text{ M}$. We show that linear Debye-Hückel-type theories do not describe even part of these data. By contrast, the Netz-Orland and Trizac-Shen formulas, two approximate theories including nonlinear electrostatic effects and the finite DNA radius, fit our data with divalent and monovalent ions, respectively, over the whole I range. Furthermore, the metallic ion type does not influence $L_P(I)$, in contrast to alkyl ammonium monovalent ions at high I .

DOI: 10.1103/PhysRevLett.122.028102

The experimental and theoretical study of polyelectrolyte stiffness has been an active field of research in the past 40 years [1–8] because its potential implications in biology, biophysics, and biotechnologies are tremendous. The diverse ionic conditions existing in the intracellular surroundings, in terms of both ionic strength and ion species [9–11], impact most of the biological macromolecules, particularly the double-stranded DNA (dsDNA), which bears one of the highest negative linear density of charges among biopolymers ($2e^-$ per base pair). In nanotechnological applications, salt conditions determine the capacity of self-assembling of single-stranded DNA as well as the mechanical properties of the resulting nanostructures [12,13], e.g., DNA origami [14–17] or aptamers [18]. Even though various fields of science are concerned, how ionic conditions influence dsDNA stiffness remains controversial from a physical perspective. Stiffness is quantified by the bending persistence length L_P , the tangent-tangent correlation length, which has two contributions: a bare one, $L_P^0 = K/(k_B T)$, related to the bending modulus K [19], and an electrostatic one associated with electrostatic repulsion within the polyelectrolyte, which is partially screened as its surrounding is enriched in counterions. As a result, L_P decreases when ion concentration grows; however, strong discrepancies exist between various experimental results obtained with different techniques [20,21], notably in force-free conditions [20] or in stretching experiments [7,22]. Furthermore, as discussed below, theoretical approaches struggle with providing a consensual frame embracing the whole range of ionic conditions.

Accurate experimental quantifications of these L_P changes are indeed nontrivial as the data analysis is not usually straightforward [20]. Recently, we have established a methodology based on high-throughput tethered particle

motion [HTTPM, see Fig. 1(a)], in which a high density of individual dsDNA molecules are tethered to a micro-patterned surface by one of their extremities, while the other one is labeled with a submicrometer-sized nanoparticle [23]. Tracking the nanoparticles thus allows us the monitoring of the conformational dynamics of single dsDNA in almost force-free conditions [24]. Following a procedure of analysis based on statistical physics modeling, we established a rigorous method to retrieve L_P from the rms of the projected end-to-end distance of the tethered particles, R_{expt} [25], and quantify its decrease as a function of the ionic strength, $I = \frac{1}{2} \sum_i z_i^2 c_i$, with z_i the valence (in units of the elementary charge e) and c_i the concentration of ion i (see Fig. 1).

From a theoretical perspective, the popular Odijk-Skolnick-Fixman (OSF) model [1,2] assimilates the polyelectrolyte to an infinitely thin and rigid rod with a uniform linear density of charges A^{-1} ($= 6e/\text{nm}$ for dsDNA where e is the elementary charge). The mobile ions, regarded as pointlike, organize in space according to the Boltzmann distribution, where the electrostatic potential is determined by linearizing the mean-field Poisson-Boltzmann (PB) equation, in the Debye-Hückel approximation valid for low electrostatic potentials. The OSF theory leads to

$$L_P = L_P^0 + \frac{\ell_B}{4A^2\kappa^2}, \quad (1)$$

where $\kappa = (8\pi\ell_B I)^{1/2}$ is the Debye parameter, and $\ell_B = e^2/(4\pi\epsilon\epsilon_0 k_B T) \simeq 0.7 \text{ nm}$ at 20°C in water is the Bjerrum length. Because of the hypothesis of low electrostatic potential, OSF theory is only valid for high I , typically above 0.1 M . At low I , a correction to the OSF model was proposed by Manning [3], where part of the ions condense

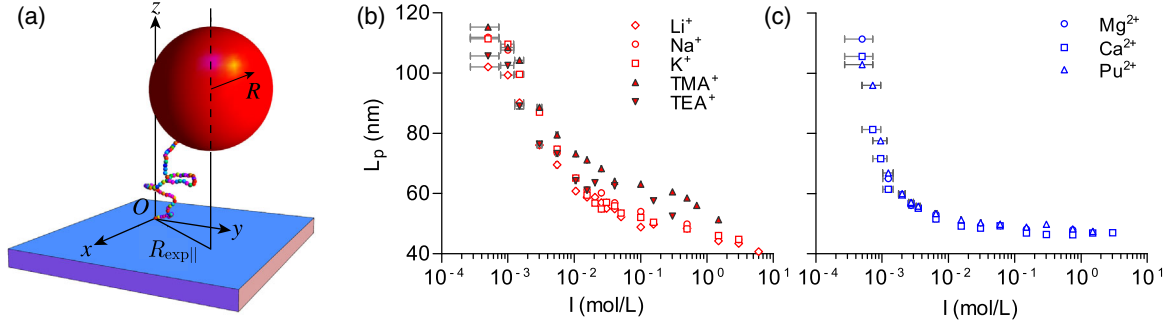


FIG. 1. (a) Sketch of the tethered particle motion setup. The measured quantity is $R_{\text{expt||}}$. Right: Influence of the ionic strength on the mean persistence length of a 1201-bp DNA for (b) monovalent and (c) divalent cations. Error bars are displayed, if not, they are smaller than the symbol size, including vertical bars (see SM Table IV [26]).

along the DNA so that the distance between the unscreened DNA elementary charges increases up to $z\ell_B$. The resulting OSF-Manning (OSFM) model leads to

$$L_P(I) = L_P^0 + \alpha^2(z) \frac{\ell_B}{4A^2\kappa^2}, \quad (2)$$

where the effective fraction of charges along the DNA $\alpha = A/(z\ell_B)$ depends on z . In order to embrace the whole range of I explored experimentally, a model developed by Netz and Orland (NO) [34] and adapted in Ref. [20] is based on a variational approximation of the full PB equation. This NO theory leads to a more complicated effective charge $\alpha(z, \kappa R_{\text{DNA}})$ that depends on the DNA radius R_{DNA} and grows with I . Finally, in 2016, Trizac and Shen (TS) corrected the OSFM formula by taking into account the first term in an expansion in κR_{DNA} of the electrostatic potential, and interpolating between exact solutions of the PB equation (in the limits of zero and high salt) for the effective charge of the DNA ξ_{eff} , that also varies with κR_{DNA} [35]. Valid only for monovalent ions, it yields the same form as Eq. (2) with α replaced by $\alpha = [(A\xi_{\text{eff}})/\ell_B](1 + \kappa R_{\text{DNA}})^{1/2}$. Hence, the TS formula differs from the NO one by the corrective term and the expression of the effective charge (computed variationally in the NO approach).

In Ref. [20], data were obtained following this HTTPM procedure with Na^+ and Mg^{2+} ranging from 10 mM to 3 M and 0.3 M, respectively. The first three models were used to fit the data. The OSF and OSFM models could not account quantitatively for the whole experimental data set obtained with Na^+ or Mg^{2+} . For the range of I studied, a reasonable scaling interpolation of the NO factor was $\alpha \propto (\kappa R_{\text{DNA}})^{\beta(z)}$, where $\beta(z)$ is an effective exponent. The NO approach could then fit the Mg^{2+} data only, while the Manning stretching model [36], which incorporates the internal stretching of the polymer modified by ion screening, succeeded in fitting the Na^+ data only.

In this Letter, challenging further the existing theories predicting $L_P(I)$, we examine a 1201-bp dsDNA [26] (i) on an extended range of I down to 0.5 mM and up to 6 M (under

well-controlled $p\text{H}$ comprised between 7 and 7.3) and (ii) with a variety of ions with different ion-specific characteristics (such as radius or hydrophobicity), neglected in all the existing theories [37] (see Fig. 1). We took much care to evaluate the influence of a large set of biologically and biotechnologically relevant ions: Li^+ , Na^+ , K^+ , tetramethyl ammonium TMA^+ , tetraethyl ammonium TEA^+ , Mg^{2+} , Ca^{2+} , putrescine Put^{2+} [see Supplemental Material (SM), Table I [26]]. We confirm that neither the OSF theory nor its Manning refinement (OSFM) describe even part of the data. By contrast, the NO model and the TS one are shown to fit accurately the data obtained with the chosen divalent and monovalent ions, respectively, and up to $I = 1$ M, with reasonable values for the fitting parameters L_P^0 and R_{DNA} . We therefore demonstrate in this work that the radii of metallic ions do not influence L_P except in the case of large alkyl ammonium monovalent ions, for which a distinct L_P^0 at high salt is obtained.

To explore the influence of ions with this extended range of I on $R_{\text{expt||}}$, we thoroughly considered the buffer composition and the influence of $p\text{H}$, which is often neglected. We became aware that, even at the usual concentration of phosphate buffer, $p\text{H}$ decreased when ions were added (see SM Fig. 1 [26] and Ref. [38]). This occurred moderately for monovalent ions but quite dramatically for divalent ions (for $I > 0.5$ M). Consequently, instead of using a phosphate buffer, we chose a 4-(2-hydroxyethyl)-1-piperazineethanesulfonic acid (HEPES) buffer at 1 mM $p\text{H}$ 7.4, denoted zero-salt buffer (with a minimum ionic strength of 0.5 mM). Using it, $p\text{H}$ is maintained between 7 and 7.3. The results obtained in the presence of Na^+ do not exhibit any fall at high I , as seen in Ref. [20]; similarly, those obtained in the presence of Mg^{2+} show a much less pronounced slope. This slower decrease in $R_{\text{expt||}}$ at high I is clearly correlated with the improved $p\text{H}$ stabilization obtained in the 1-mM HEPES buffer, as we experimentally confirmed that acidic $p\text{H}$ negatively affected $R_{\text{expt||}}$ (see SM Fig. 1 [26]).

We then supplemented the zero-salt buffer with monovalent metallic ions Li^+ , Na^+ , K^+ (ionic radii ranging from

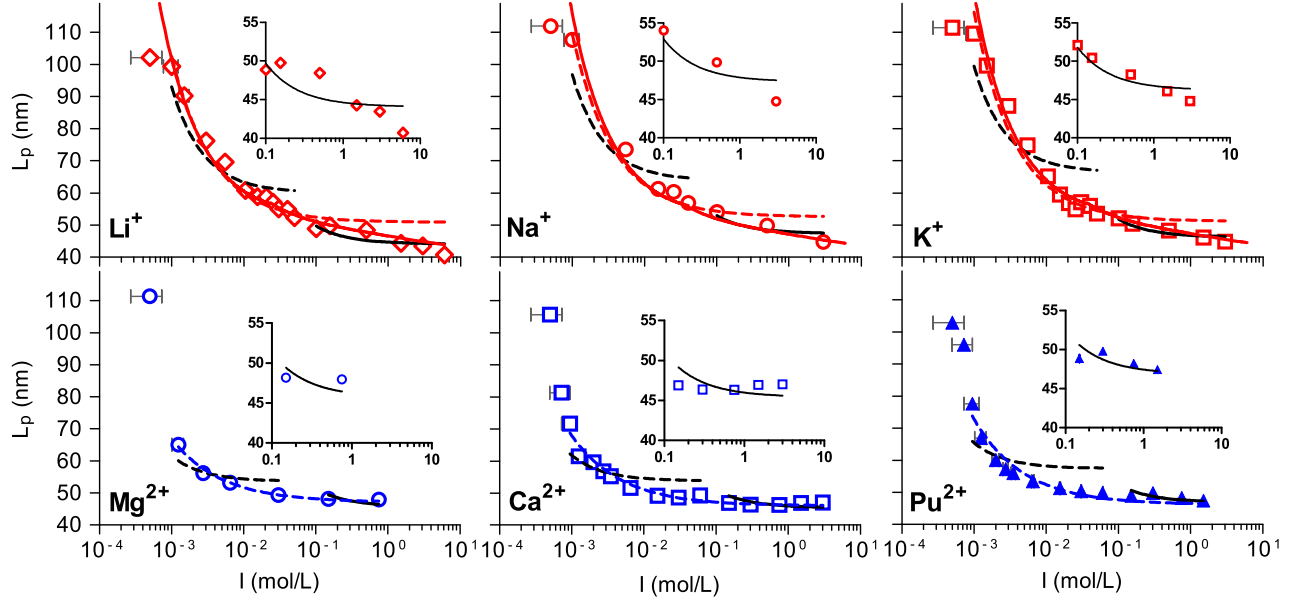


FIG. 2. Ionic strength dependence of L_p for monovalent (top, red) and divalent (bottom, blue) ions with fitting curves corresponding to OSF [$L_p(I) = L_p^0 + 0.559/I$ (nm), where I is expressed in mol/L and L_p in nm; black line], OSFM (black dashed line), NO (dashed lines), and TS (solid lines) theories. Insets are enlargements of the high I region. For monovalent ions, the NO model leads to $L_p = L_p^0 + 0.404R_{\text{DNA}}^{0.490}I^{-0.755}$ (nm) [with $\alpha = 0.635(\kappa R_{\text{DNA}})^{0.245}$ [20]]. For divalent ions, it leads to $L_p = L_p^0 + 0.238R_{\text{DNA}}^{0.728}I^{-0.636}$ (nm) [with $\alpha = 0.423(\kappa R_{\text{DNA}})^{0.364}$ [20]]. Error bars are displayed, if not, they are smaller than the symbol size, including vertical bars (see SM Table IV [26]).

0.071 to 0.141 nm) and divalent metallic ions Mg^{2+} and Ca^{2+} (ionic radii of 0.070 and 0.103 nm; see SM Table I [26]). When I increases from 0.5 mM to 3 M, $R_{\text{expt||}}$ decreases by about 20% for both types of metallic ions (SM Fig. 2 [26]). We notice a faster decrease for divalent ions. In order to consider much larger ions, we carried out experiments with three polyamines: TMA^+ , TEA^+ , and Put^{2+} (an essential metabolite of many living organisms, e.g., found at high concentration in *E. coli* [39]). TMA^+ and TEA^+ have radii 3–4 times larger than those of the chosen metallic monovalent ions. Put^{2+} size has not been characterized yet; however, its radius likely exceeds that of the metallic ions. Surprisingly, in the case of divalent ions, $R_{\text{expt||}}$ values are extremely similar for both metallic ions and Put^{2+} . In the presence of TMA^+ and TEA^+ , they are significantly higher than those obtained with metallic monovalent ions.

From $R_{\text{expt||}}$, we extracted L_p using calibration curves obtained by exact sampling simulation based on a statistical physics model of DNA [20]. As expected, L_p decreases much faster when I increases in the presence of divalent ions than in the presence of monovalent ions. Unexpectedly, the data superimpose on a unique curve for the three divalent ions [Fig. 1(c)] but not for the five monovalent ones [Fig. 1(b)]. In addition, L_p reaches a plateau above $I \approx 50$ mM for the divalent ions while, in the case of monovalent ions, only a shoulder at $I \approx 200$ mM can be detected within the continuously decreasing curve. Molecular dynamics simulations examining the role of Na^+ identified a similar transitory plateau followed by a fall at high salt (SM Fig. 5

[26]) [21,40]. Moreover, we have measured that in the presence of monovalent ions at $I \approx 150$ mM, adding even only 1-mM divalent ions leads to a significant decrease of ≈ 6 nm in L_p (SM Fig. 4 [26]). This demonstrates an additive effect of monovalent and divalent ions at these biologically relevant ion concentrations.

To determine which theory best describes our experimental results, we performed fits with four equations corresponding to the OSF, OSFM, NO, and TS models. Fitting parameters are L_p^0 , and in addition, for NO and TS models, R_{DNA} . The fitting curves are displayed in detail in Fig. 2 and fitting parameter values and standard deviation of the residuals are given in SM Tables II and III [26]. Both OSF and OSFM formulas yield very poor fits for the whole I range (see SM [26]). Since the OSF formula is theoretically valid at high salt, we fitted the data for $I \geq 100$ mM. We observed discrepancies for monovalent ions, due to the absence of saturation in the experimental data. For divalent ions, the fit is correct but only for this small range of I . For $I \leq 100$ mM, fits of L_p using the OSFM equation were equivalently inadequate for monovalent and divalent ions. We then employed the NO model on the entire I range, excluding the very first points at low I that may be partially biased due to possible plastic tube contamination (see SM section “Material and methods” [26]) but could strongly contribute to the fit due to their high L_p value, exceeding 100 nm. For the divalent ions, we observed extremely good adjustments of $L_p(I)$ by the NO fits (with $46 \leq L_p^0 \leq 47$ nm) with very good values of the standard deviation of

the residuals (see SM Table II [26]). For monovalent ions, the NO fits seem reasonable at low salt (for $1 \leq I \leq 30$ mM) but systematically overestimate $L_p(I)$ at high salt. Moreover, the fitting values for R_{DNA} are small, only half the expected size of 1 nm. To circumvent this discrepancy as well as the poor fitting at high salt, we considered the TS analytical formula [35], which considerably improved the $L_p(I)$ fit as observed in Fig. 2 (see SM Table III [26]). Note that the fitted value $L_p^0 = 41$ nm is the same for the three metallic ions and slightly smaller than the divalent's one (fitted with a different theory), and R_{DNA} is almost constant, between 0.85 and 1 nm. The strong agreement at high I comes from the precise expression of ξ_{eff} at large ionic strength [41]. The NO variational theory, on the other hand, looks for the optimized formula $\alpha(\kappa R_{\text{DNA}})$ for the whole I range, at the expense of this high precision for large I , where its limiting behavior is, by construction, the OSF formula. For the TMA⁺ and TEA⁺ ions the value of L_p^0 is slightly higher (51 and 47 nm, respectively), which could be correlated to their large size (see SM Table I [26]).

On the basis of the TS theory, we can also explore the combined effects of the temperature T and the ionic strength I on L_p on structurally intact dsDNA. In a previous work, the effect of the temperature has been measured experimentally at fixed physiological salt conditions, $I = 160$ mM [42]. It has been shown that L_p decreases as $1/T$ as expected from the simple formula valid for neutral wormlike chains $L_p^0 = K/(k_B T)$. However, not only the bare persistence length L_p^0 but also the electrostatic contribution depends on T , since entropic effects control the ionic screening of the dsDNA. Hence, using our fitting values obtained at $T = 20$ °C, we plotted $L_p(T)$ for various I in Fig. 3. We observed that for $I \geq 100$ mM, the electrostatic contribution is small as compared to L_p^0 . Therefore, we observe a $1/T$ law with a shift of the curve to lower values when I increases. For $I < 4$ mM, however, we predict a striking reversal with L_p increasing with T .

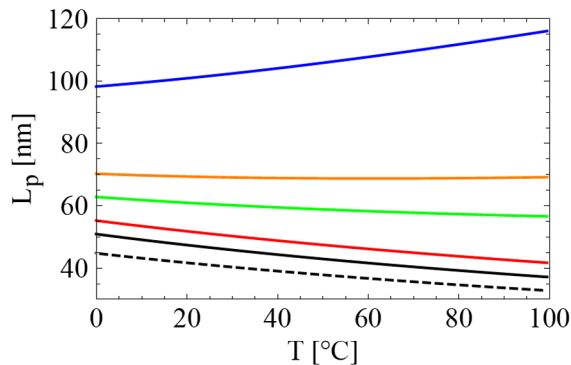


FIG. 3. Theoretical prediction of the influence of the temperature T on L_p for monovalent ions and $I = 0.001, 0.004, 0.01, 0.1, 1$ M from top to bottom. The dashed curve is the infinite I limit showing the nonelectrostatic contribution $L_p^0 = K/(k_B T)$.

New experiments exploring the dependence of the L_p as a function of T and I are therefore needed to check further the theoretical TS approach.

No influence of the size or the nature of the ions was seen as the curves obtained with the three divalent ions and the three metallic monovalent ions superimposed in two unique curves. This complete superimposition prevents us from considering as significant the slight changes of dsDNA radius derived from the fits. The independence of the ionic-strength variation of L_p with the ion size and our fitted values for $R_{\text{DNA}} \approx 1$ nm are in good agreement with the experimental results of Gebala and co-workers [43]. They showed that the atmosphere occupancy around dsDNA by monovalent ions did not depend on the ion size across the monovalent metallic ions except for Li⁺ [43], which only led to a slight reduction as compared to the other monovalent metallic ions. These two distinct approaches thus support the same view of an identical behavior for various metallic monovalent ions with different sizes. Therefore, in timescales of seconds, the differences in the ion binding sites along the DNA tube [44] and residence times [45] measured between Na⁺ and K⁺ using molecular dynamic simulations of tens of nanoseconds fade away.

Concerning alkyl ammonium ions, their significantly higher L_p^0 suggests that their 3–4 times wider ion size precludes a sufficiently large density of ions close to dsDNA to completely screen the electrostatic interactions, even at large I . The capacity of these ions to easily dehydrate and consequently enter the dsDNA grooves, as predicted by molecular dynamic simulations [46], is insufficient to screen the dsDNA charges. Hydrated divalent metallic ions such as Mg²⁺ were predicted to exhibit a much more localized distribution than Na⁺ and K⁺ and to spend long resident times of a few nanoseconds within the dsDNA tube [45]; yet, we did not measure any impact on the fitted R_{DNA} value. Surprisingly, Put²⁺ behaves as metallic divalent ions in spite of its long linear structure. This is at odds with what was found to describe thermal DNA denaturation in the presence of Put²⁺ [39,47].

The great efficiency of NO and TS theories comes from the consideration of nonlinear electrostatic terms and of the finite radius of dsDNA. It suggests that they could also be valid for other polyelectrolytes. For hyaluronic acid in the presence of Na⁺ in stretching experiments with magnetic tweezers [49], L_p decreases following $L_p = L_p^0 + \text{const} \times I^{-\delta}$ with $\delta = 0.65$ at low salt to be compared with our value of 0.75, while L_p^0 is about 10 times shorter than the dsDNA one, and the charge density is 6 times smaller. The use of NO and TS theories to finely model the flexibility of biopolymers such as single-stranded RNA [50] or chromatin fibers should be extremely useful for the elucidation of gene expression and 3D organization of chromosomes [51] and for the control of the shape of nucleic acid nanostructures [52].

We acknowledge Philippe Rousseau (LMGM, CBI, Toulouse) for the DNA samples.

* manghi@irsamc.ups-tlse.fr

† tardin@ipbs.fr

‡ Present address: Department of Physics, University of York, York YO10 5DD, United Kingdom.

- [1] T. Odijk, Polyelectrolytes near the rod limit, *J. Polym. Sci.* **15**, 477 (1977).
- [2] J. Skolnick and M. Fixman, Electrostatic persistence length of a Wormlike polyelectrolyte, *Macromolecules* **10**, 944 (1977).
- [3] G. S. Manning, A procedure for extracting persistence lengths from light-scattering data on intermediate molecular weight DNA, *Biopolymers* **20**, 1751 (1981).
- [4] M. Fixman, The flexibility of polyelectrolyte molecules, *J. Chem. Phys.* **76**, 6346 (1982).
- [5] M. Le Bret, Electrostatic contribution to the persistence length of a polyelectrolyte, *J. Chem. Phys.* **76**, 6243 (1982).
- [6] J.-L. Barrat and J.-F. Joanny, Persistence length of polyelectrolyte chains, *Europhys. Lett.* **24**, 333 (1993).
- [7] C. Baumann, S. Smith, V. Bloomfield, and C. Bustamante, Ionic effects on the elasticity of single DNA molecules, *Proc. Natl. Acad. Sci. U.S.A.* **94**, 6185 (1997).
- [8] J. Wenner, M. Williams, I. Rouzina, and V. Bloomfield, Salt dependence of the elasticity and overstretching transition of single DNA molecules, *Biophys. J.* **82**, 3160 (2002).
- [9] K. Fagerbakke, M. Heldal, and S. Norland, Content of carbon, nitrogen, oxygen, sulfur and phosphorus in native aquatic and cultured bacteria, *Aquatic Microbial Ecology* **10**, 15 (1996).
- [10] M. Heldal, S. Norland, and O. Tumor, X-Ray microanalytical method for measurement of dry matter and elemental content of individual bacteria, *Appl. Environ. Microbiol.* **50**, 1251 (1985).
- [11] B. Alberts, A. Johnson, J. Lewis, M. Raff, K. Roberts, and P. Walter, *Molecular Biology of the Cell*, 4th ed. (Garland Science, New York, 2002).
- [12] S. H. Lee, C. K. Lee, S. R. Shin, S. I. Kim, I. So, and S. J. Kim, The peculiar response of DNA hydrogel fibers to a salt and pH stimulus, *Macromol. Rapid Commun.* **30**, 430 (2009).
- [13] J. D. Halverson and A. V. Tkachenko, DNA-programmed mesoscopic architecture, *Phys. Rev. E* **87**, 062310 (2013).
- [14] S. Fischer, C. Hartl, K. Frank, J. O. Rädler, T. Liedl, and B. Nickel, Shape and Interhelical spacing of DNA origami nanostructures studied by small-angle x-ray scattering, *Nano Lett.* **16**, 4282 (2016).
- [15] R. P. Goodman, I. A. Schaap, C. F. Tardin, C. M. Erben, R. M. Berry, C. F. Schmidt, and A. J. Turberfield, Rapid chiral assembly of rigid DNA building blocks for molecular nanofabrication, *Science* **310**, 1661 (2005).
- [16] A. Reinhardt and D. Frenkel, Numerical Evidence for Nucleated Self-Assembly of DNA Brick Structures, *Phys. Rev. Lett.* **112**, 238103 (2014).
- [17] F. Hong, F. Zhang, and H. Yan, DNA Origami: Scaffolds for creating higher order structures, *Chem. Rev.* **117**, 12584 (2017).
- [18] K. Padmanabhan, K. P. Padmanabhan, J. D. Ferrara, J. E. Sadler, and A. Tulinsky, The structure of alpha-thrombin inhibited by a 15-mer single-stranded DNA aptamer, *J. Biol. Chem.* **268**, 17651 (1993).
- [19] O. Kratky and G. Porod, Röntgenuntersuchung gelöster Fadenmoleküle, *Recl. Trav. Chim.* **68**, 1106 (1949).
- [20] A. Brunet, C. Tardin, L. Salomé, P. Rousseau, N. Destainville, and M. Manghi, Dependence of DNA persistence length on ionic strength of solutions with monovalent and divalent salts: A joint theory-experiment study, *Macromolecules* **48**, 3641 (2015).
- [21] A. Savelyev, Do monovalent mobile ions affect DNAs flexibility at high salt content?, *Phys. Chem. Chem. Phys.* **14**, 2250 (2012).
- [22] O. A. Saleh, D. B. McIntosh, P. Pincus, and N. Ribeck, Nonlinear Low-Force Elasticity of Single-Stranded DNA Molecules, *Phys. Rev. Lett.* **102**, 068301 (2009).
- [23] T. Plenat, C. Tardin, P. Rousseau, and L. Salomé, High-throughput single-molecule analysis of DNA-protein interactions by tethered particle motion, *Nucl. Acids Res.* **40**, e89 (2012).
- [24] D. E. Segall, P. C. Nelson, and R. Phillips, Volume-Exclusion Effects in Tethered-Particle Experiments: Bead Size Matters, *Phys. Rev. Lett.* **96**, 088306 (2006).
- [25] M. Manghi, C. Tardin, J. Baglio, P. Rousseau, L. Salomé, and N. Destainville, Probing DNA conformational changes with high temporal resolution by tethered particle motion, *Phys. Biol.* **7**, 046003 (2010).
- [26] See Supplemental Material at <http://link.aps.org/supplemental/10.1103/PhysRevLett.122.028102> for the material and methods, experimental issues, a comparison to existing simulation results, and the fitting procedure, which includes Refs. [27–33].
- [27] J. R. Rossum, Conductance method for checking accuracy of water analyses, *Anal. Chem.* **21**, 631 (1949).
- [28] S. Blumberg, A. Gajraj, M. W. Pennington, and J.-C. Meiners, Three-dimensional characterization of tethered microspheres by total internal reflection fluorescence microscopy, *Biophys. J.* **89**, 1272 (2005).
- [29] A. Brunet, S. Chevalier, N. Destainville, M. Manghi, P. Rousseau, M. Salhi, L. Salomé, and C. Tardin, Probing a label-free local bend in DNA by single molecule tethered particle motion, *Nucl. Acids Res.* **43**, e72 (2015).
- [30] Y. Marcus, Ionic radii in aqueous solutions, *Chem. Rev.* **88**, 1475 (1988).
- [31] J. M. G. Barthel, H. Krienke, and W. Kunz, *Physical Chemistry of Electrolyte Solutions: Modern Aspects* (Springer Science & Business Media, New York, 1998).
- [32] L. A. Yatsunyk, O. Mendoza, and J.-L. Mergny, “Nano-oddities”: Unusual nucleic acid assemblies for DNA-based nanostructures and nanodevices, *Acc. Chem. Res.* **47**, 1836 (2014).
- [33] P. Bevington and D. K. Robinson, *Data Reduction and Error Analysis for the Physical Sciences* (McGraw-Hill Education, New York, 2003).
- [34] R. R. Netz and H. Orland, Variational charge renormalization in charged systems, *Eur. Phys. J. E* **11**, 301 (2003).
- [35] E. Trizac and T. Shen, Bending stiff charged polymers: The electrostatic persistence length, *Europhys. Lett.* **116**, 18007 (2016).
- [36] G. S. Manning, The contribution of transient counterion imbalances to DNA bending fluctuations, *Biophys. J.* **90**, 3208 (2006).
- [37] G. S. Manning (private communication).

- [38] C. M. H. Ferreira, I. S. S. Pinto, E. V. Soares, and H. M. V. M. Soares, (Un)suitability of the use of *pH* buffers in biological, biochemical and environmental studies and their interaction with metal ions—a review, *RSC Adv.* **5**, 30989 (2015).
- [39] L. Miller-Fleming, V. Olin-Sandoval, K. Campbell, and M. Ralser, Remaining mysteries of molecular biology: The role of polyamines in the cell, *J. Mol. Biol.* **427**, 3389 (2015).
- [40] A. Savelyev and G. A. Papoian, Chemically accurate coarse graining of double-stranded DNA, *Proc. Natl. Acad. Sci. U.S.A.* **107**, 20340 (2010).
- [41] M. Aubouy, E. Trizac, and L. Bocquet, Effective charge versus bare charge: An analytical estimate for colloids in the infinite dilution limit, *J. Phys. A* **36**, 5835 (2003).
- [42] A. Brunet, L. Salomé, P. Rousseau, N. Destainville, M. Manghi, and C. Tardin, How does temperature impact the conformation of single DNA molecules below melting temperature?, *Nucl. Acids Res.* **46**, 2074 (2018).
- [43] M. Gebala, S. Bonilla, N. Bisaria, and D. Herschlag, Does cation size affect occupancy and electrostatic screening of the nucleic acid ion atmosphere?, *J. Am. Chem. Soc.* **138**, 10925 (2016).
- [44] P. Várnai and K. Zakrzewska, DNA and its counterions: A molecular dynamics study, *Nucl. Acids Res.* **32**, 4269 (2004).
- [45] F. Pan, C. Roland, and C. Sagui, Ion distributions around left- and right-handed DNA and RNA duplexes: A comparative study, *Nucl. Acids Res.* **42**, 13981 (2014).
- [46] D. Bhowmik, N. Malikova, G. Mériguet, O. Bernard, J. Teixeira, and P. Turq, Aqueous solutions of tetraalkylammonium halides: Ion hydration, dynamics and ion-ion interactions in light of steric effects, *Phys. Chem. Chem. Phys.* **16**, 13447 (2014).
- [47] Our measurements are performed on 1201-bp-long DNA molecules for which any sequence effect [44,48] is assumed to be self-averaged.
- [48] S. Y. Ponomarev, K. M. Thayer, and D. L. Beveridge, Ion motions in molecular dynamics simulations on DNA, *Proc. Natl. Acad. Sci. U.S.A.* **101**, 14771 (2004).
- [49] J. P. Berezney and O. A. Saleh, Electrostatic effects on the conformation and elasticity of Hyaluronic acid, a moderately flexible polyelectrolyte, *Macromol.* **50**, 1085 (2017).
- [50] H. Chen, S. P. Meisburger, S. A. Pabit, J. L. Sutton, W. W. Webb, and L. Pollack, Ionic strength-dependent persistence lengths of single-stranded RNA and DNA, *Proc. Natl. Acad. Sci. U.S.A.* **109**, 799 (2012).
- [51] G. Zhu, W. Deng, H. Hu, R. Ma, S. Zhang, J. Yang, J. Peng, T. Kaplan, and J. Zeng, Reconstructing spatial organizations of chromosomes through manifold learning, *Nucl. Acids Res.* **46**, e50 (2018).
- [52] P. Liu, Y. Zhao, X. Liu, J. Sun, D. Xu, Y. Li, Q. Li, L. Wang, S. Yang, C. Fan *et al.*, Charge neutralization drives the shape reconfiguration of DNA nanotubes, *Angew. Chem.* **57**, 5418 (2018).